

Optical properties of circular photonic crystal fibers filled with carbon tetrachloride

Hoang Trong Duc¹, Le Tran Bao Tran², Tran Ngoc Thao², Chu Van Lanh²,
Nguyen Thi Thuy^{1,*}

¹University of Education, Hue University, 34 Le Loi, Hue City, Thua Thien Hue province,
Viet Nam

²Department of Physics, Vinh University, 182 Le Duan, Vinh City, Nghe An province, Viet Nam

*Email: ntthuy@hueuni.edu.vn

Received: 4 April 2022; Accepted for publication: 29 March 2023

Abstract. In this work, the dispersion properties and nonlinear properties of circular photonic crystal fibers were improved by a combination of carbon tetrachloride infiltration into the core and modification of the air hole diameters d_1 and d_2 of rings in the cladding. The quantities such as dispersion, effective mode area, nonlinear coefficient, and low confinement are analyzed in detail. Based on the survey results, two photonic crystal fibers with optimal optical properties were proposed which are beneficial for supercontinuum generation. The first fiber with $\Lambda = 1.0$ μm , $d_1/\Lambda = 0.6$, has an all-normal dispersion of -10.785 ps/nm.km at a pump wavelength of 0.985 μm . The high nonlinear coefficient of 581.795 $\text{W}^{-1}.\text{km}^{-1}$ and the low confinement loss of 3.904 dB/m are also achieved with this fiber. SC broadband under the influence of soliton is expected to be generated when using the second fiber ($\Lambda = 2.0$ μm , $d_1/\Lambda = 0.3$) with flat and low anomalous dispersion at the pump wavelength of 1.3 μm .

Keywords: photonic crystal fiber, circular lattice, nonlinearity coefficient, effective mode area, confinement loss, supercontinuum generation.

Classification numbers: 2.1.1.

1. INTRODUCTION

Photonic crystal fiber (PCF) is a hot topic attracting the attention of many research groups since it was published in the 90s [1] until now. Thanks to the flexible design, it is possible to adjust the optical properties like birefringent, nonlinearity, mode area, confinement loss, zero-dispersion, etc. [2 - 5]. There are many ways to design PCFs suitable for different applications such as selection of air hole size, shape, lattice constant, substrate material or replacing completely or alternative materials are the popular methods to control dispersion and achieve the expected nonlinear properties [6 - 8] because dispersion and nonlinear effects dominate supercontinuum (SC) generation in optical fibers. A large number of fibers have been studied to explore PCF's ability to generate better SC generation due to their ability to adjust optical properties. Thus, PCF is currently one of the best nonlinear mediums for SC generation.

The nonlinear effects that occur when a pump pulse propagates in the PCF are strongly influenced by its dispersion properties. SC expansion is strongly promoted by high-order soliton separation if the fiber is injected in the anomalous dispersion region, close to the zero-dispersion wavelength. Unfortunately, the coherence of the obtained SC is relatively low [9, 10] even though the spectrum expands very broadly, which leads to limitations in some application areas such as medicine, metrology, and optical pulse compression [11, 12]. Meanwhile, self-phase modulation and optical breaking are the main mechanisms governing the spectral broadening when the fiber is pumped in the all-normal dispersion regime. Although the bandwidth is smaller, the spectrum is flatter and has good coherence because soliton-related phenomenon does not affect the spectrum [13 - 15].

In recent years, many research groups have found effective improvement of the dispersion characteristics of PCF filled by high nonlinear refractive index liquids, this effort aims to further improve the efficiency of the SC generation process. An all-normal or anomalous dispersion, flat dispersion, and low confinement loss in liquid-filled PCFs can be achieved by varying the size of the air holes and the number of air-hole layers in the cladding, respectively. PCFs filled with liquids with high nonlinear refractive index: ethanol [16], methanol [17], carbon disulfide [18], chloroform [19], benzene [20], nitrobenzene [21], tetrachloroethylene [22], toluene [23] provided a flat dispersion resulting in a broad SC spectrum, however, the effective mode area is still large, the nonlinear coefficient is relatively low and the confinement loss has not yet reached the desired value. These limitations are not beneficial for the SC generation process.

In this paper, we choose carbon tetrachloride to fill the hollow core of PCF because of the following reasons: First, its toxicity is relatively low compared to some other liquids such as carbon disulfide or toluene [24]. Second, the nonlinear refractive index of carbon tetrachloride is 5 times higher than that of fused silica [25]. Third, the linear refractive index of carbon tetrachloride is approximately equal to that of silica, which makes the coupling compatible between the PCF-filled carbon tetrachloride fiber and the silica fiber highly efficient resulting in a single-mode fiber. The circular lattice is also remarkable in the design because the high symmetry leads to the highest concentration of electromagnetic field energy in the core. Along with the new structural design emphasizing the difference between the air hole diameters of the first ring near the core and the other rings in the cladding, we have obtained both all-normal and anomalous dispersion properties with multiple zero dispersion wavelengths (ZDWs), small dispersion values are also observed. Furthermore, nonlinear quantities such as effective mode area, nonlinear coefficient, and confinement loss have been found to have reasonable values as expected. The advantages of PCF with carbon tetrachloride infiltration are perfectly suitable for SC generation application in all-fiber laser systems.

2. NUMERICAL MODELING

A new carbon tetrachloride filled-PCF structure with eight layers of air holes distributed periodically in a circular pattern and running along the PCF length as depicted in Figure 1(a). The diameter of air holes in the first and the other rings are denoted as d_1 and d_2 , respectively. The center to center distance of holes is lattice constant and represented by Λ . In our design, the difference in diameters of the first and other rings of air holes was carefully chosen to achieve a flat dispersion, small, and prevent attenuation. This comes from the idea introduced by works [6, 26 - 28] that the dispersion optimization even the shift of ZDW is strongly influenced by the air hole size of the innermost ring while the other rings dominate nonlinear properties especially the attenuation of fundamental mode or even higher modes. So, we varied the filling factor d_1/Λ of the innermost ring near the core in the range of 0.3 to 0.8 but the d_2/Λ of other rings is kept

constant at 0.95. We choose the lattice constants of PCF that are $\Lambda = 1.0, 1.5, 1.8,$ and $2.0 \mu\text{m}$ to investigate the variation of characteristic quantities on this parameter. The hollow large core of PCFs is infiltrated with carbon tetrachloride and has the diameter $D_c = 2\Lambda - 1.1d_1$, which helps to increase the ability to confine light into the core, thereby enhancing the nonlinearity of PCFs with such structural design, we have obtained PCFs with the modes of the electromagnetic field held in the core. Figure 1(b) presents that the intensity distribution is confined on the core of PCF with $\Lambda = 2.0 \mu\text{m}$, $d_1/\Lambda = 0.65$.

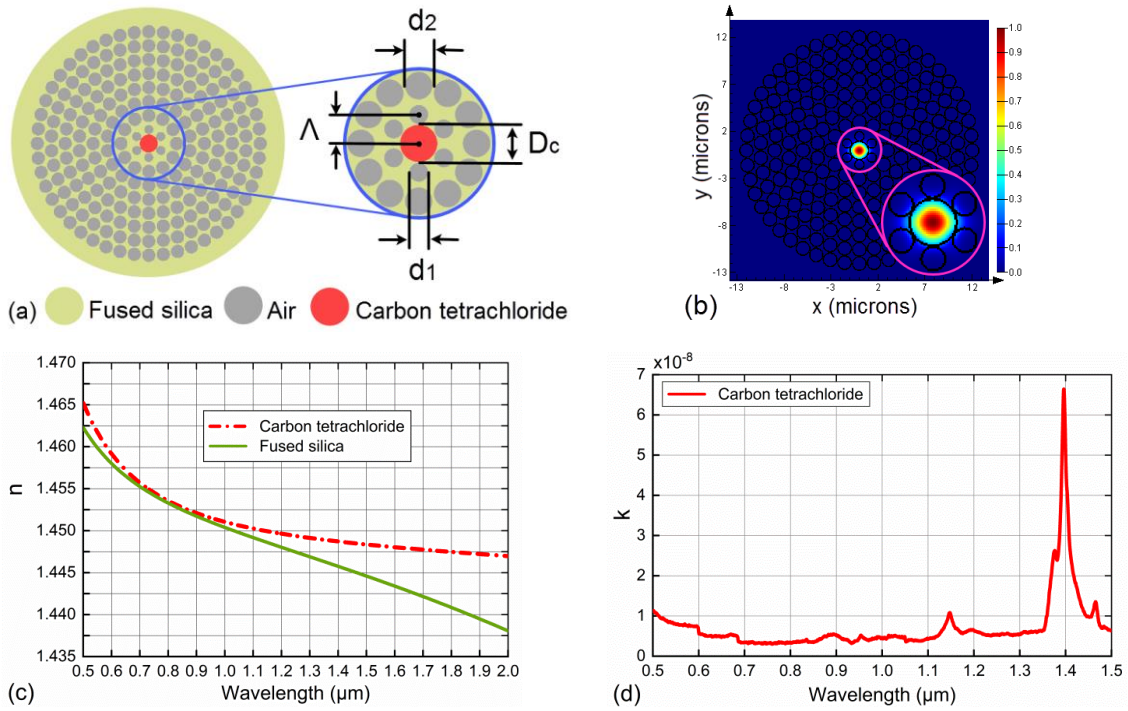


Figure 1. Cross-section view of geometric structure (a), intensity distribution in the PCF filled with carbon tetrachloride with $\Lambda = 1.5 \mu\text{m}$, $d_1/\Lambda = 0.65$ (b), the real parts of the refractive index n of carbon tetrachloride and fused silica is extrapolated using Cauchy's equation and Sellmeier's equation (c), and the imaginary k part of the refraction index of carbon tetrachloride based on experimental data from [29] (d).

Figure 1(c) shows the dependence of real parts of the refractive index n of carbon tetrachloride and fused silica on wavelength. It can see that the linear refractive index of CCl_4 is low and close to that of fused silica in the lower wavelength region from 0.5 to $1.1 \mu\text{m}$. This value is slightly higher than that of fused silica in the larger wavelength region. Cauchy's equation [30] and Sellmeier's equation [31] described the relationship between the refractive index characteristics and wavelength for CCl_4 and fused silica.

$$n_{\text{CCl}_4}^2(\lambda) = 2.085608282 + 0.00053373\lambda^2 + \frac{0.012201206}{\lambda^2} + \frac{0.000056451}{\lambda^4} + \frac{0.000048106}{\lambda^6} \quad (1)$$

$$n_{\text{SiO}_2}^2(\lambda) = 1 + \frac{0.6961663\lambda^2}{\lambda^2 - (0.0684043)^2} + \frac{0.4079426\lambda^2}{\lambda^2 - (0.1162414)^2} + \frac{0.8974794\lambda^2}{\lambda^2 - (9.896161)^2} \quad (2)$$

where λ is the excitation wavelength in micrometers, $n(\lambda)$ is the wavelength-dependent linear refractive index of materials.

The imaginary k part of the refractive index of carbon tetrachloride for the temperature of 20 °C, based on experimental data from [29] is displayed in Figure 1(d). There are an absorption peaks at about 1.148 μm and the strongest absorption peak at 1.396 μm with k reaching the value of 6.677×10^{-8} , corresponding to the attenuation ($a = 10 \cdot \log [e^{4\pi k/\lambda}]$ [23]) at this wavelength is equal to 32.13 dB/cm. We also assumed that fiber losses are only contribution from material loss of CCl_4 , as shown in Figure 2(b). Thus, the fibers have a high loss in long wavelengths (i.e., $\lambda > 1.4 \mu\text{m}$).

The propagation of the fundamental mode can be simulated by the full-vector finite-difference eigenmode (FDE) method using Lumerical Mode Solutions (LMS) software. The spatial profile and frequency dependence of modes are solved by Maxwell's equations on a cross-sectional mesh of the waveguide to obtain the mode field profiles, effective index, dispersion, and loss with assuming a significant loss of carbon tetrachloride. The wavelength ranges from 0.6 to 2.0 μm due to the reliable data range.

3. RESULTS AND DISCUSSION

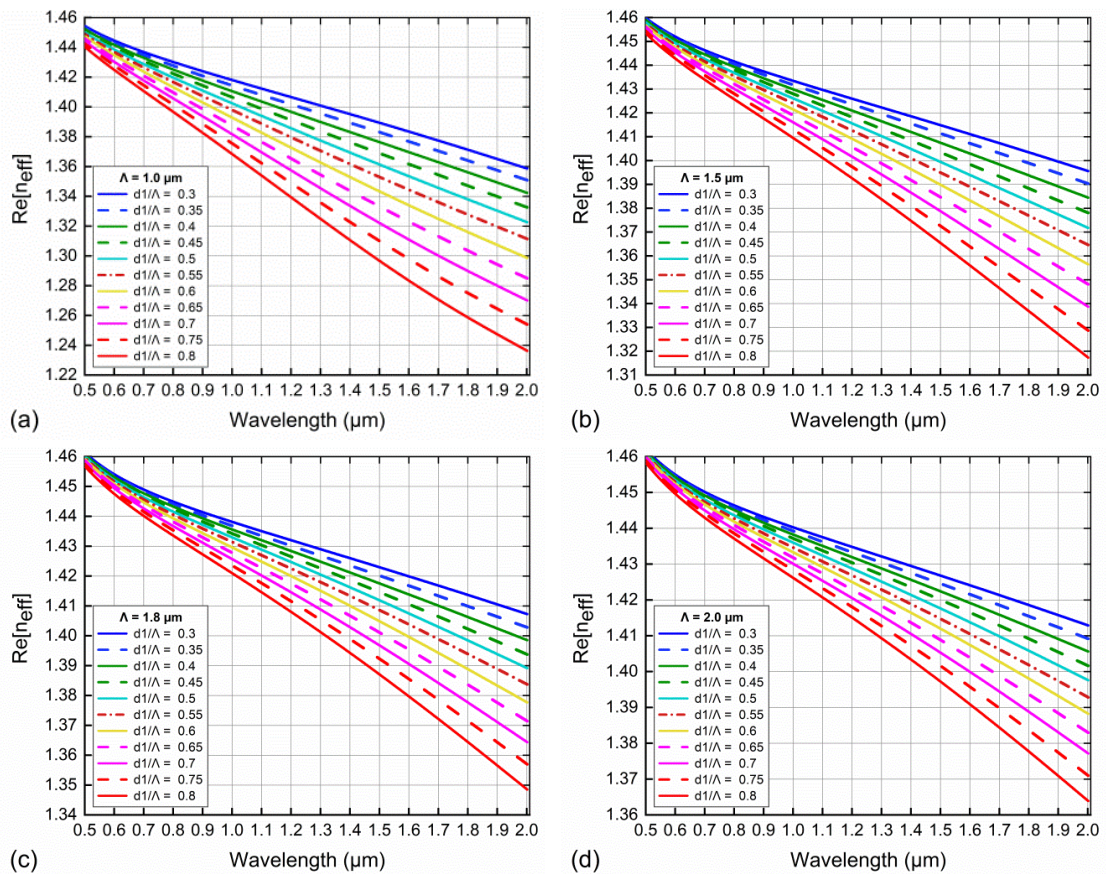


Figure 2. The real part of effective refractive index as a function of wavelength of PCFs with various d_1/Λ for (a) $\Lambda = 1.0 \mu\text{m}$, (b) $\Lambda = 1.5 \mu\text{m}$, (c) $\Lambda = 1.8 \mu\text{m}$ and (d) $\Lambda = 2.0 \mu\text{m}$.

The real part of the effective refractive index ($\text{Re}[n_{\text{eff}}]$) for the fundamental mode versus wavelength in the range of 0.5 - 2 μm has presented in Figure 2. Increasing the wavelength

reduces the $\text{Re}[n_{\text{eff}}]$ gradually, and their curve is similar for all cases of d_1/Λ and Λ . This behavior is mainly the result of a stronger penetration of longer wavelengths into the cladding of PCFs than shorter wavelengths [32]. Moreover, the variation of d_1/Λ and Λ also strongly influences the effective refractive index. At a certain value of wavelength, the $\text{Re}[n_{\text{eff}}]$ decreases with increasing d_1/Λ for each instance of Λ . Conversely, as Λ rises, it increases for each fixed d_1/Λ resulting in a progressively smaller slope of the effective refractive index curves. The reason for this is the greater enlargement of the core, as well as the larger contribution than that of fused silica in the cladding refractive index [24].

Table 1 indicates the value of $\text{Re}[n_{\text{eff}}]$ of fibers with different Λ and d_1/Λ calculated at a wavelength of 1.55 μm . We obtain the maximum and minimum values of $\text{Re}[n_{\text{eff}}]$ of 1.425 and 1.29 for the cases $\Lambda = 2.0 \mu\text{m}$, $d_1/\Lambda = 0.3$ and $\Lambda = 1.0 \mu\text{m}$, $d_1/\Lambda = 0.8$, respectively.

Table 1. The real part of the effective refractive index of PCFs with various Λ and d_1/Λ at 1.55 μm wavelength.

d_1/Λ	$\text{Re}[n_{\text{eff}}]$			
	$\Lambda = 1.0 (\mu\text{m})$	$\Lambda = 1.5 (\mu\text{m})$	$\Lambda = 1.8 (\mu\text{m})$	$\Lambda = 2.0 (\mu\text{m})$
0.3	1.386	1.413	1.421	1.425
0.35	1.380	1.409	1.418	1.423
0.4	1.373	1.405	1.416	1.421
0.45	1.365	1.401	1.413	1.418
0.5	1.357	1.397	1.410	1.416
0.55	1.349	1.392	1.406	1.413
0.6	1.339	1.387	1.402	1.410
0.65	1.328	1.381	1.398	1.406
0.7	1.316	1.375	1.394	1.403
0.75	1.304	1.368	1.389	1.399
0.8	1.290	1.361	1.383	1.394

In the case of ultra-short pulse propagation, the chromatic dispersion determines the extent to which different spectral components travel with different velocities in the PCF. Nonlinear processes will be dominant and be able to generate new frequencies in the pulse spectrum if dispersion around the pump wavelength is minimized, so we can obtain a broadband supercontinuum. The chromatic dispersion has numerically calculated through the effective refractive index n_{eff} dependence, given by the formula below [33]:

$$D = -\frac{\lambda}{c} \frac{d^2 \text{Re}[n_{\text{eff}}]}{d\lambda^2} \tag{3}$$

where c is the speed of light in a vacuum.

The effect of the air hole diameter d_1 and lattice constant Λ on the dispersion properties of PCFs is illustrated in Figure 3. It is clear from Figure 3(a) that the dispersion properties change significantly on changing the filling factor d_1/Λ when Λ is fixed. Thus, it seems very convenient to get desired dispersion characteristic of structure using d_1 . For the case $\Lambda = 1.0$, the dispersion properties were found quite diverse including all-normal dispersion and anomalous dispersion with one or two ZDWs.

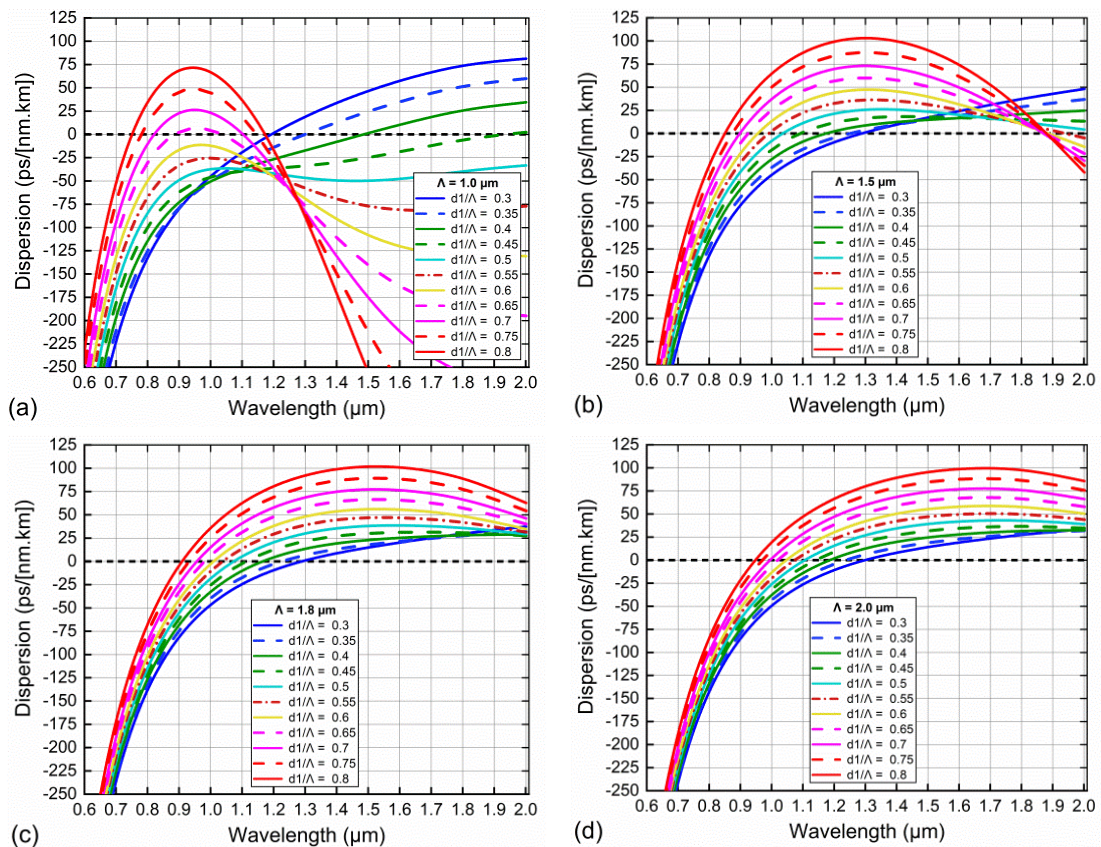


Figure 3. The dispersion as a function of wavelength of PCFs with various d_1/Λ for (a) $\Lambda = 1.0 \mu\text{m}$, (b) $\Lambda = 1.5 \mu\text{m}$, (c) $\Lambda = 1.8 \mu\text{m}$ and (d) $\Lambda = 2.0 \mu\text{m}$.

This allows us many opportunities to choose structures with optimal dispersion for SC. Interestingly, dispersion against the increase of d_1/Λ in the longer wavelength region (greater than $1.2 \mu\text{m}$) but increases with d_1/Λ in the shorter wavelength region, leading to an increase in the slope of the dispersion curves. Anomalous dispersion with one ZDW is observed for d_1/Λ less than 0.5. Furthermore, the ZDWs shift towards the longer wavelength. When d_1/Λ varies from 0.65 to 0.8, we achieve anomalous dispersions with two ZDWs, which means that the dispersion is divided into three regions where the normal dispersion is on the shorter and longer wavelength sides. Three all-normal dispersions corresponding to $d_1/\Lambda = 0.5, 0.55, 0.6$ have been found in the investigated wavelength region. All-normal dispersions are also the goal of many research groups in generating SC with a broad, high coherence, and flat spectrum. The lattice constant Λ also strongly dominates the dispersion properties of PCFs, specifically when Λ increases to $1.5 \mu\text{m}$, the all-normal dispersion curves are lifted above the zero-dispersion to become anomalous dispersion with two ZDWs. Besides, the anomalous dispersion curves with $d_1/\Lambda = 0.3 - 0.5$ are flatter and closer to zero dispersion than that for the case $\Lambda = 1.0 \mu\text{m}$ (Figure 3(b)). As Λ increases further, only anomalous dispersion exists with one ZDW and it shifts towards shorter wavelengths with an increase of d_1/Λ (Figures 3(c) and (d)).

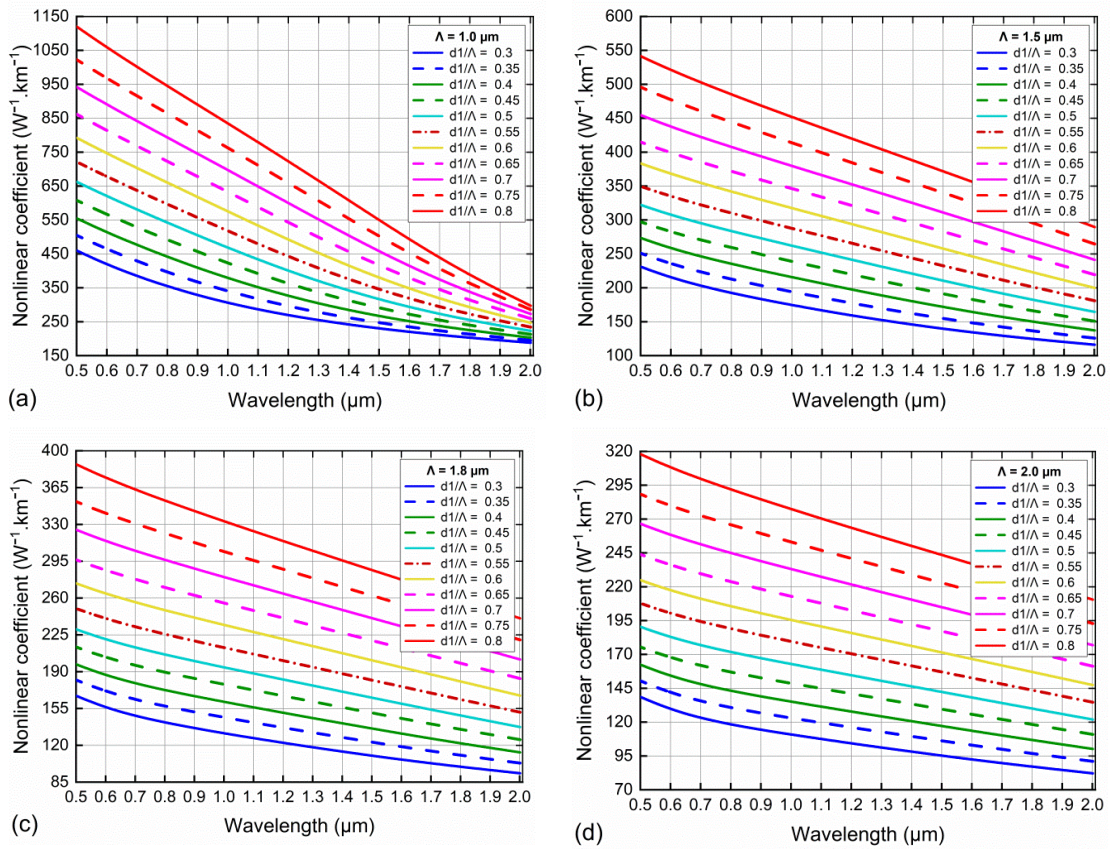


Figure 4. The nonlinear coefficient as a function of wavelength of PCFs with various d_1/Λ for (a) $\Lambda = 1.0 \mu\text{m}$, (b) $\Lambda = 1.5 \mu\text{m}$, (c) $\Lambda = 1.8 \mu\text{m}$ and (d) $\Lambda = 2.0 \mu\text{m}$.

The nonlinear coefficient is one of the important factors originating from the interaction of intense light with the matter due to the Kerr effect. The general numerical expression of frequency-dependent Kerr nonlinearity [33] exhibits the relationship of the linear refractive index, nonlinear refractive index, and effective mode area of the fundamental mode as given below:

$$\gamma(\lambda) = 2\pi \frac{n_2}{\lambda A_{\text{eff}}} \tag{4}$$

where A_{eff} is the effective mode area, a key parameter in designing PCFs. It determines the extent of the electromagnetic field confinement in the core of the PCF, which can be calculated using [34] with E as the amplitude of the transverse electric field propagating inside the PCF.

$$A_{\text{eff}} = \frac{\left(\iint |E|^2 dx dy \right)^2}{\iint |E|^4 dx dy} \tag{5}$$

The nonlinear coefficient going from high value to low value corresponding to the decrease of effective mode area with increasing wavelength has shown in Figures 4 and 5. In the case of Λ fixed, the values of the nonlinear coefficient increased, and the effective mode area of the fundamental mode is found to decrease with the increase of the filling factor d_1/Λ .

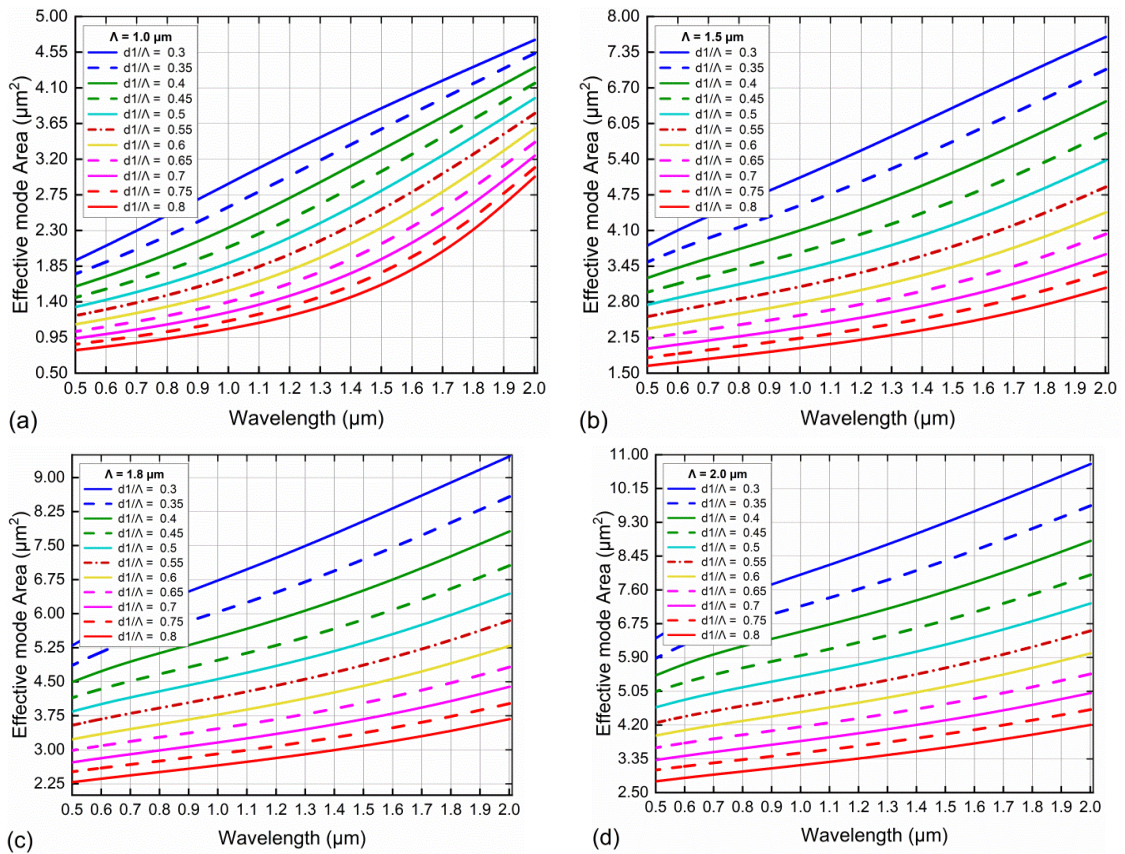


Figure 5. The effective mode area as a function of wavelength of PCFs with various d_1/Λ for (a) $\Lambda = 1.0 \mu\text{m}$, (b) $\Lambda = 1.5 \mu\text{m}$, (c) $\Lambda = 1.8 \mu\text{m}$ and (d) $\Lambda = 2.0 \mu\text{m}$.

Table 2. The nonlinearity coefficients ($\text{W}^{-1} \cdot \text{km}^{-1}$) and the effective mode areas (μm^2) PCFs with various Λ and d_1/Λ at $1.55 \mu\text{m}$ wavelength.

d_1/Λ	$\Lambda = 1.0 (\mu\text{m})$		$\Lambda = 1.5 (\mu\text{m})$		$\Lambda = 1.8 (\mu\text{m})$		$\Lambda = 2.0 (\mu\text{m})$	
	γ	A_{eff}	γ	A_{eff}	γ	A_{eff}	γ	A_{eff}
0.3	225.295	3.932	136.925	6.468	108.282	8.179	93.850	9.436
0.35	240.892	3.678	151.433	5.849	120.886	7.326	104.628	8.464
0.4	258.889	3.423	167.958	5.274	133.584	6.630	115.402	7.674
0.45	281.061	3.153	186.863	4.741	148.234	5.974	127.697	6.935
0.5	304.665	2.91	205.728	4.306	162.499	5.450	140.254	6.314
0.55	331.756	2.673	227.203	3.899	178.948	4.949	154.887	5.717
0.6	363.655	2.439	251.921	3.516	197.551	4.483	169.108	5.236
0.65	397.269	2.234	276.533	3.203	216.092	4.098	184.657	4.795
0.7	435.992	2.036	304.203	2.912	237.094	3.735	202.162	4.380
0.75	477.275	1.860	332.759	2.662	258.258	3.429	219.956	4.026
0.8	521.461	1.703	363.852	2.434	282.127	3.139	240.246	3.686

The small core exhibits better light confinement of the core leading to an increase in the nonlinearity coefficient and a decrease in the effective mode area, respectively since these two

values are inversely proportional to each other. The increase of the lattice constant (larger cores) reduces the nonlinear coefficient leading to an increase in the effective mode area. Among the surveyed structures, the maximum and minimum values of the nonlinear coefficient at the wavelength of 1.55 μm (which are common commercial laser wavelength) were observed to be 521.461 $\text{W}^{-1}.\text{km}^{-1}$ and 93.85 $\text{W}^{-1}.\text{km}^{-1}$ for the cases $A = 1.0 \mu\text{m}$, $d_1/A = 0.8$ and $A = 2.0 \mu\text{m}$, $d_1/A = 0.3$, respectively. Similarly, with these two structures, we achieve the maximum and minimum values of the effective mode area of 1.703 μm^2 and 9.436 μm^2 , respectively. The values of the nonlinearity coefficients and the effective mode areas at the 1.55 μm of the PCFs filled with CCl_4 are shown in Table 2.

Confinement losses are the losses arising from the leaky nature of the modes and it depends on the wavelength computed from the imaginary part of the effective refractive index $\text{Im}[n_{\text{eff}}(\lambda)]$ of the PCF by [34]

$$L_c = 8.686 \frac{2\pi}{\lambda} \text{Im}[n_{\text{eff}}(\lambda)]. \tag{6}$$

For a small A , the relatively low confinement losses represent good light restriction in the core of the PCFs. The confinement loss has a larger value in the longer wavelength region, the leakage of modes at low frequency occurs not only in the core of the PCFs but also in the core and cladding regions. Otherwise, the variation of d_1/A strongly affects the confinement loss, which decreases as d_1/A increases (Figure 6). The value of confinement loss increases rapidly as A increases, it is clear that larger cores can reduce the leakage potential of the guide modes. The values of L_c at 1.55 μm are indicated in Table 3. L_c has the maximum value up to 74.257 dB/m for the structure $A = 1.0 \mu\text{m}$, $d_1/A = 0.3$ and reaches the minimum value of 19.86 dB/m with $A = 2.0 \mu\text{m}$, $d_1/A = 0.75$.

Table 3. The confinement loss of PCFs with various A and d_1/A at 1.55 μm wavelength.

d_1/A	L_c (dB/m)			
	$A = 1.0 (\mu\text{m})$	$A = 1.5 (\mu\text{m})$	$A = 1.8 (\mu\text{m})$	$A = 2.0 (\mu\text{m})$
0.3	74.257	50.522	40.839	35.947
0.35	72.527	47.345	37.315	32.600
0.4	70.328	43.701	34.168	29.706
0.45	67.664	40.163	31.031	26.866
0.5	65.750	38.049	29.231	25.045
0.55	63.172	35.457	27.118	23.034
0.6	60.415	32.865	25.105	21.471
0.65	58.120	31.182	23.901	20.701
0.7	55.680	29.799	22.909	19.926
0.75	53.371	29.056	22.667	19.860
0.8	51.473	28.763	22.666	19.989

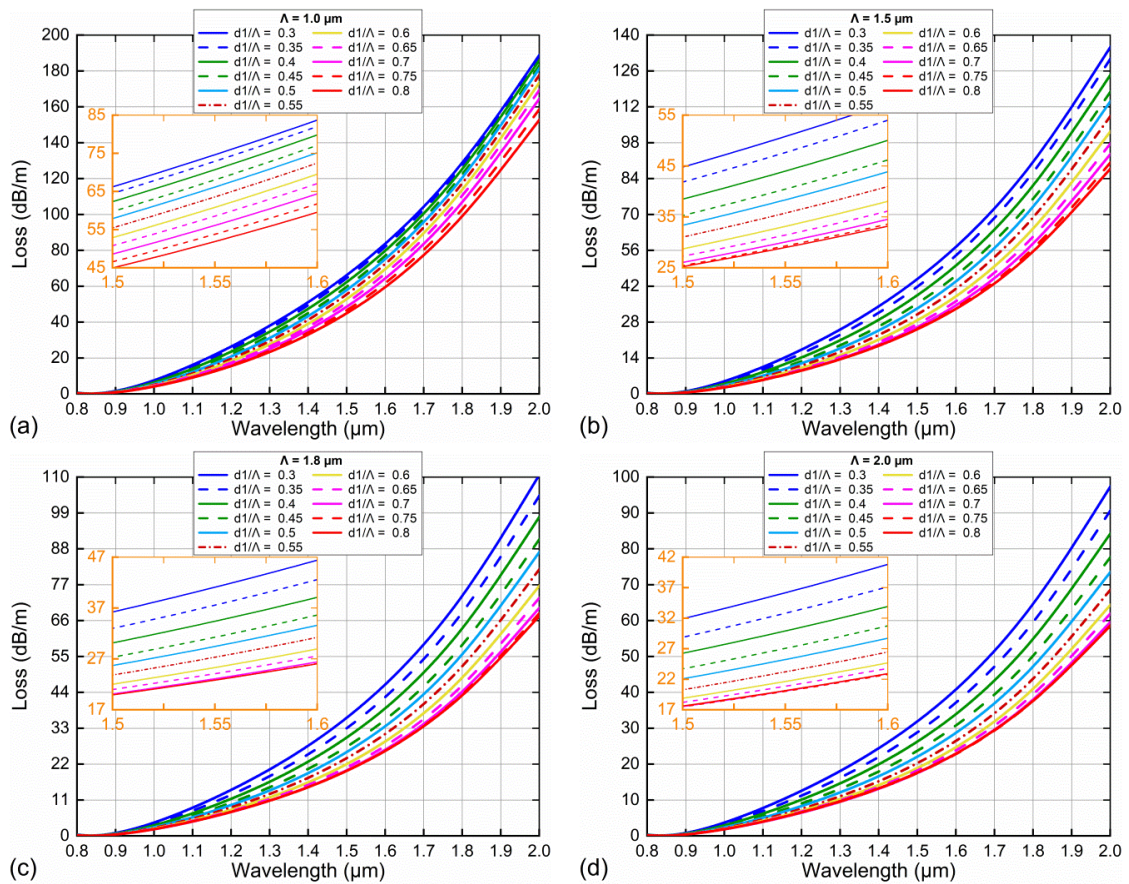


Figure 6. The confinement loss as a function of wavelength of PCFs with various d_1/Λ for (a) $\Lambda = 1.0 \mu\text{m}$, (b) $\Lambda = 1.5 \mu\text{m}$, (c) $\Lambda = 1.8 \mu\text{m}$ and (d) $\Lambda = 2.0 \mu\text{m}$.

A PCF with suitable dispersion characteristics has been an important factor governing the efficiency of SC generation since the variation in optical pulse per unit distance of the propagation length of the fiber is affected by dispersion. The optical properties results from the above numerical simulation show that dispersion properties and its flatness are controlled more effectively by the combination of tuning the d_1 parameter of the innermost ring and the penetration of CCl_4 to the core of PCF. We select two optimal PCFs to benefit the generation SC, called #F₁ and #F₂ with the following lattice parameters: $\Lambda = 1.0 \mu\text{m}$, $d_1/\Lambda = 0.6$ (#F₁) and $\Lambda = 2.0 \mu\text{m}$, $d_1/\Lambda = 0.3$ (#F₂). They have small dispersion and reasonable flatness that can use in SC generation, displayed in figure 7. With the all-normal dispersion regime of fiber $\Lambda = 1.0 \mu\text{m}$, $d_1/\Lambda = 0.6$, the pump wavelength can select near the maximum point of the dispersion curve, so we choose the pump wavelength for this structure to be $0.985 \mu\text{m}$. Together with a small dispersion of -10.785 ps/nm.km at the pump wavelength, we expect to obtain a high coherence and flatter SC spectrum. For $\Lambda = 2.0 \mu\text{m}$, $d_1/\Lambda = 0.3$, the anomalous dispersion curve is the flattest and closest to the zero-dispersion, with a dispersion value of 0.287 ps/nm.km at the $1.3 \mu\text{m}$ pump wavelength, this fiber will give a broader soliton fission-based SC spectrum with lower input energy. We obtained a smaller dispersion value at the pump wavelength than in some previous papers on PCF filled with other liquids [19 - 23].

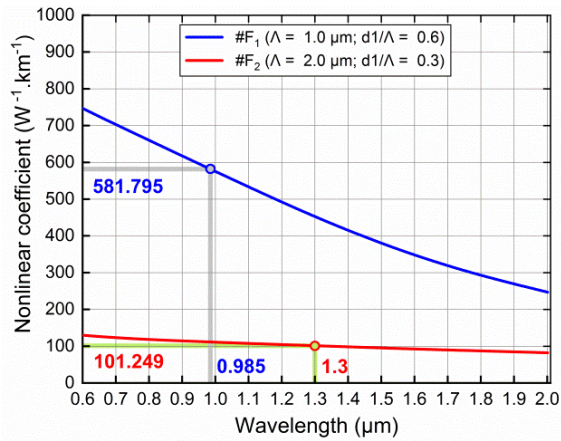


Figure 8. The nonlinear coefficient of #F₁ and #F₂ optimal fiber.

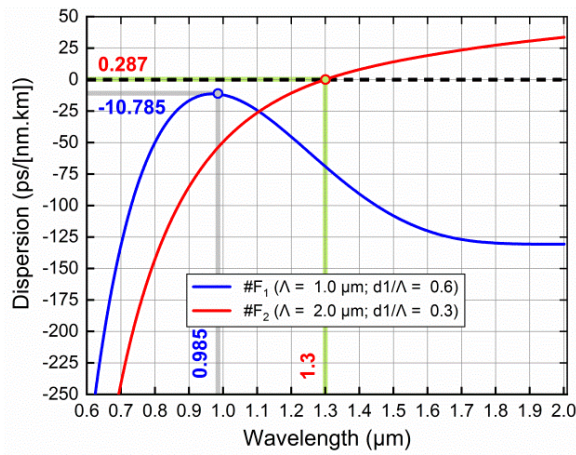


Figure 7. The dispersion characteristics of #F₁ and #F₂ optimal fiber.

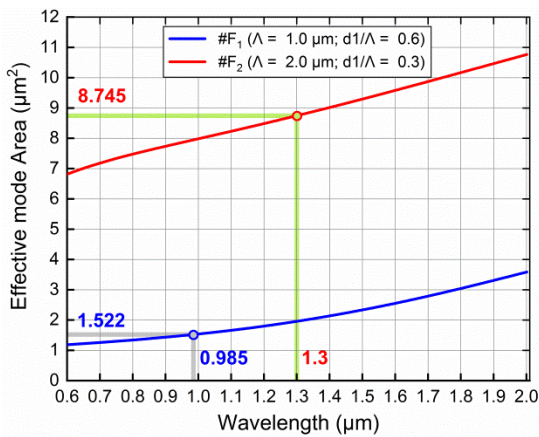


Figure 9. The effective mode area of #F₁ and #F₂ optimal fiber.

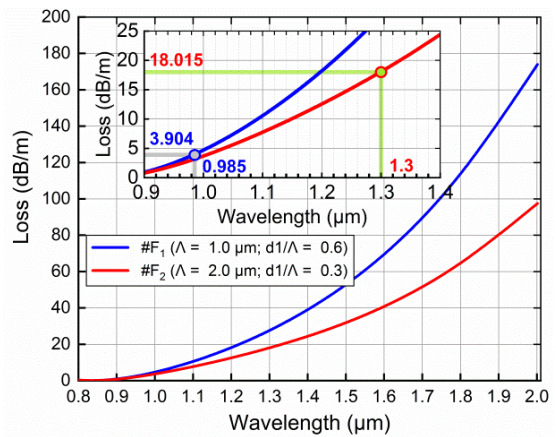


Figure 10. The confinement losses of #F₁ and #F₂ optimal fiber.

For two fibers with reasonable dispersion introduced above, we consider their nonlinear coefficients and effective mode areas to evaluate their applicability in SC generation. The nonlinearity coefficient is quite high and the effective mode area is as low as desired at the pumping wavelength of the all-normal dispersion regime fiber #F₁ of 581.795 W⁻¹.km⁻¹ and 1.522 μm², respectively. Whereas #F₂ fiber exhibiting anomalous dispersion achieves lower values of the nonlinear coefficient and higher values of effective mode area, which are 101.249 W⁻¹.km⁻¹ and 8.745 μm², respectively. Because of the different dispersion properties, the two fibers have different nonlinear coefficients and different effective mode areas, but the values are very suitable for SC generation. The high nonlinear coefficients enable this optimized fiber-based SC generation to have a low input power that can be as low as nano joules. The parameters characterizing the nonlinear properties of the proposed fibers are more optimal than some PCFs infiltrated with other high nonlinear coefficient liquids [20, 23, 24]. These are also the outstanding advantages of the PCFs in our research.

The selection of air holes size and core size gives us to achieve low values of confinement loss, the values of L_c at the pump wavelength are 3.904 dB/m and 18.015 dB/m of #F₁ and #F₂ fiber. Although the #F₂ fiber has a larger confinement loss, it has low dispersion and high nonlinear coefficient, so the ability to generate broad-spectrum SC based on the soliton effect is completely possible. We have calculated confinement losses for the PCF. The losses are similar to the ones calculated for an ideal structure. Because the confinement loss of the two optimal fibers is quite low at the pump wavelength, they have a small contribution to the fiber loss during SC generation. Fiber losses are mainly from the contribution of material losses of CCl₄ but these fibers have low losses in the short wavelength range (less than 1.4 μm). Therefore, in our model, we assume that the fiber losses in the long wavelength range have a value of 31.2 dB/cm.

Table 4. The structure parameters and the characteristic quantities of optimal PCFs at the pump wavelength compared with other publications on liquids-infiltrated PCFs.

#	D_c (μm)	Λ (μm)	d_1/Λ	Pump wavelength (μm)	A_{eff} (μm ²)	γ (W ⁻¹ .km ⁻¹)	D (ps/nm.km)	L_c (dB/m)
#F ₁	1.34	1.0	0.6	0.985	1.522	581.795	-10.785	3.904
#F ₂	3.34	2.0	0.3	1.3	8.745	101.249	0.287	18.015
#F ₁ [36], CCl ₄	2.25	1.5	0.45	1.35	11.83	-	12	1.85
#F ₂ [36], CCl ₄	7.12	4.0	0.8	1.064	10.58	-	-4.37	1.58
#I_0.3 [23], C ₇ H ₈	6.56	2.0	0.3	1.55	7.79	2132.575	-7.784	40
#I_0.35 [23], C ₇ H ₈	5.6	2.0	0.5	1.55	78.9	2890.276	-1.19	120
#F ₁ [19], CHCl ₃	3.37	1.0	0.65	1.03	1.5	1290	-24	-
#F ₂ [19], CHCl ₃	3.285	2.0	0.65	1.03	4.48	440	7.6	-
#F ₁ [22], C ₂ Cl ₄	1.28	1.5	0.4	1.56	433.2	156.9	-15	4.0
#F ₂ [22], C ₂ Cl ₄	3.753	4.0	0.45	1.56	16.67	40.79	3.2	4.2
#F ₃ [22], C ₂ Cl ₄	1.198	1.5	0.55	1.03	359.1	189.3	-4.85	5.3

In the next study, when optimal fibers are used for SC, the losses of fibers will be taken into account in our model although the effect of fiber losses may not be evident during spectrum

expansion. Because of the high non-linear refractive index of CCl_4 it can allow a wide spectrum of SC to be generated in a short propagation (several centimeters). However, we note that the maximum loss of 3.2 dB/cm present at 1.4 μm may have an influence on degradation of SG dynamic. So, only a short segment of the fiber should be used for SC generation to minimize this effect [35]. Table 4 indicates the structure parameters and the characteristic quantities of optimal PCFs at the pump wavelength compared with other publications on liquids-infiltrated PCFs.

In experiment, some other publications also show that the ability to generate SC with broad spectra by using high nonlinear liquids-infiltrated PCFs. By the conventional stack-and-draw method [36], PCFs can be easily fabricated in the experiment. The liquids are filled into the core by integrating a microfluidic pump system using a thermal fusion splicer or laser writing technique [37]. “A fusion splicer to close air holes in the photonic cladding was used. The thermal method was applied to collapse air holes in the cladding of developed PCF. The fiber is heated in the middle using single short electrical pulse, in order to collapse selectively only holes in the photonic cladding and leave the hollow core open” [35]. The liquids infiltration process of the developed fiber with collapsed cladding air holes was based on capillary forces [38]. This method further verifies that PCFs filled with liquid have great potential in practical applications.

4. CONCLUSIONS

By modifying the structural parameters of PCF combined with core filling with a high nonlinear coefficient carbon tetrachloride liquid which notices the difference in hole diameters in the first ring nearest to the core and the other rings, we have achieved optimal nonlinear characteristics including dispersion, nonlinear coefficient, effective mode area, and confinement loss. Among the designed fibers, we have selected and analyzed in detail two structures with the flattest dispersion, closest to the zero-dispersion. The first fiber has an all-normal dispersion with a value of -10.785 ps/nm.km at a pump wavelength of 0.985 μm . Another advantage of this fiber is its small effective mode area and high nonlinear coefficient, suggesting for SC generation with low peak power. With anomalous dispersion profile, the second fiber gives a low dispersion value of 0.287 ps/nm.km at a pump wavelength of 1.3 μm , which is expected to produce a broad SC spectrum through soliton dynamics. Two optimal PCFs can be the new optical fiber replacing the traditional glass core fiber to improve the efficiency of the SC generation.

Acknowledgements. This research is funded by Vietnam National Foundation for Science and Technology Development (NAFOSTED) under grant number 103.03-2020.03 and Vietnam’s Ministry of Education and Training (B2021-DHH-08).

CRedit authorship contribution statement. Hoang Trong Duc: Writing manuscript, Plotting graph. Le Tran Bao Tran, Tran Ngoc Thao: Design and simulate the PCFs structures. Chu Van Lanh: Methodology, Data analysis, Supervision. Nguyen Thi Thuy: Data processing, Manuscript editing, Supervision.

Declaration of competing interest. The authors declare that they have no known competing financial interests or personal relationships that could have appeared to influence the work reported in this paper.

REFERENCES

1. Dudley J. M., Genty G., and Coen S. - Supercontinuum generation in photonic crystal fiber, Review of Modern Physics **78** (4) (2006) 1135-1184. <https://doi.org/10.1103/RevModPhys.78.1135>.

2. Nair A. A., Amiri I.S., Boopathi C. S., Karthikumar S., Jayaraju M., and Yupapin P. - Numerical investigation of co-doped microstructured fiber with two zero dispersion wavelengths, *Results in Physics* **10** (2018) 766-771. <https://doi.org/10.1016/j.rinp.2018.07.032>.
3. Hou J., Zhao J., Yang C., Zhong Z., Gao Y., and Chen S. - Engineering ultra-flattened-dispersion photonic crystal fibers with uniform holes by rotations of inner rings, *Photonics Research* **2** (2) (2014) 59-63. <https://doi.org/10.1364/PRJ.2.000059>.
4. Borgohain N., Sharma M., and Konar S. - Broadband supercontinuum generation in photonic crystal fibers using cosh-Gaussian pulses at 835 nm wavelength, *Optik* **127** (4) (2016) 1630-1634. <http://dx.doi.org/10.1016/j.ijleo.2015.11.063>.
5. Lanh C. V., Thuy N. T., Bao Tran L. T., Duc H. T., Ngoc V. T. M., Hieu V. L., and Van T. H. - Multi-octave supercontinuum generation in As₂Se₃ chalcogenide photonic crystal fiber, *Photonics and Nanostructures - Fundamentals and Applications* **48** (2022) 100986. <https://doi.org/10.1016/j.photonics.2021.100986>.
6. Thuy N. T., Duc H. T., Bao Tran L. T., Trong D. V., and Lanh C. V. - Optimization of optical properties of toluene-core photonic crystal fibers with circle lattice for supercontinuum generation, *Journal of Optics* (2022). <https://doi.org/10.1007/s12596-021-00802-y>.
7. Liao J., Wang Z., Huang T., Wei Q., and Li D. - Design of step-index-microstructured hybrid fiber for coherent supercontinuum generation, *Optik* **243** (2021) 167393. <https://doi.org/10.1016/j.ijleo.2021.167393>.
8. Alam M. Z., Tahmid M. I., Mouna S. T., Islam M. A., and Alam M. S. - Design of a novel star type photonic crystal fiber for mid-infrared supercontinuum generation, *Optics Communications* **500** (2021) 127322. <https://doi.org/10.1016/j.optcom.2021.127322>.
9. Petersen C. R., Prtljaga N., Farries M., Ward J., Napier B., Lloyd G. R., Nallala J., Stone N., and Bang O. - Mid-infrared multispectral tissue imaging using a chalcogenide fiber supercontinuum source, *Optics Letters* **43** (5) (2018) 999-1002. <https://doi.org/10.1364/OL.43.000999>.
10. Abeeluck A. K., and Headley C. - Continuous-wave pumping in the anomalous- and normal-dispersion regimes of nonlinear fibers for supercontinuum generation, *Optics Letters* **30** (1) (2005) 61-63. <https://doi.org/10.1364/OL.30.000061>.
11. Dudley J., and Coen S. - Fundamental limits to few-cycle pulse generation from compression of supercontinuum spectra generated in photonic crystal fiber, *Optics Express* **12**(11) (2004) 2423-2428. <https://doi.org/10.1364/OPEX.12.002423>.
12. Yi J., Chen S., Shu X., Fawzi A., and Zhang H. - Human retinal imaging using visible-light optical coherence tomography guided by scanning laser ophthalmoscopy, *Biomedical Optics Express* **6** (10) (2015) 3701-3713. <https://doi.org/10.1364/BOE.6.003701>.
13. Heidt A. M., Hartung A., Bosman G. W., Krok P., Rohwer E. G., Schwoerer H., and Bartelt H. - Coherent octave spanning near-infrared and visible supercontinuum generation in all-normal dispersion photonic crystal fibers, *Optics Express* **19** (4) (2011) 3775-3787. <https://doi.org/10.1364/OE.19.003775>.
14. Kedenburg S., Strutynski C., Kibler B., Froidevaux P., Desevedavy F., Gadret G., Jules J. C., Steinle T., Morz F., Steinmann A., Giessen H., and Smektala F. - High repetition rate mid-infrared supercontinuum generation from 1.3 to 5.3 μm in robust step-index tellurite fibers, *Journal of the Optical Society of America B* **34** (3) (2017) 601-607.

- <https://doi.org/10.1364/JOSAB.34.000601>.
15. Sinobad M., Torre A. D., Armand R., Davies B. L., Ma P., Madden S., Mitchell A., Moss D. J., Hartmann J. M., Fedeli J. M., Monat C., and Grillet C. - Mid-infrared supercontinuum generation in silicon-germanium all-normal dispersion waveguides, *Optics Letters* **45** (18) (2020) 5008-5011. <https://doi.org/10.1364/OL.402159>.
 16. Bao Tran L. T., Thuy N. T., Ngoc V. T. M., Trung L. C., Minh L. V., Van C. L., Khoa D. X., and Lanh C. V. - Analysis of dispersion characteristics of solid-core PCFs with different types of lattice in the claddings, infiltrated with ethanol, *Photonics Letters of Poland* **12** (4) (2020) 106-108. <https://doi.org/10.4302/plp.v12i4.1054>.
 17. Chauhan P., Kumar A., and Kalra Y. - Supercontinuum generation in a hollow-core methanol-silica based photonic crystal fiber: computational model and analysis, *Proc. SPIE 11498, Photonic Fiber and Crystal Devices: Advances in Materials and Innovations in Device Applications XIV*, (2020) 114980T. <https://doi.org/10.1117/12.2568970>.
 18. Sharafali A., Ali A. K. S., and Lakshmanan M. - Modulation instability induced supercontinuum generation in liquid core suspended photonic crystal fiber with cubic-quintic nonlinearities, *Physics Letters A* **399** (2022) 127290. <https://doi.org/10.1016/j.physleta.2021.127290>.
 19. Lanh C. V., Van T. H., Van C. L., Borzycki K., Khoa D. X., Vu T. Q., Trippenbach M., Buczyński R., and Pniewski J. - Optimization of optical properties of photonic crystal fibers infiltrated with chloroform for supercontinuum generation, *Laser Physics* **29** (7) (2019) 075107. <https://doi.org/10.1088/1555-6611/ab2115>.
 20. Lanh C. V., Van T. H., Van C. L., K. Borzycki, Khoa D. X., Vu T. Q., M. Trippenbach, R. Buczyński, and J. Pniewski. - Supercontinuum generation in benzene-filled hollow-core fibers, *Optical Engineering* **60**(11) (2021) 116109. <http://doi.org/10.1117/1.OE.60.11.116109>.
 21. Lanh C. V., Van T. H., Van C. L., Borzycki K., Khoa D. X., Vu T. Q., Trippenbach M., Buczyński R., and Pniewski J. - Supercontinuum generation in photonic crystal fibers infiltrated with nitrobenzene, *Laser Physics* **30**(3) (2020) 035105. <https://doi.org/10.1088/1555-6611/ab6f09>.
 22. Hieu V. L., Van T. H., Hue T. N., Van C. L., Buczynski R., and Kasztelaniec R. - Supercontinuum generation in photonic crystal fibers infiltrated with tetrachloroethylene, *Optical and Quantum Electronics* **53** (2021) 187. <https://doi.org/10.1007/s11082-021-02820-3>.
 23. Lanh C. V., Anuszkiewicz A., Ramaniuk A., Kasztelaniec R., Khoa D. X., Van C. L., Trippenbach M., and Buczyński R. - Supercontinuum generation in photonic crystal fibres with core filled with toluene, *Journal of Optics* **19** (12) (2017) 125604. <https://doi.org/10.1088/2040-8986/aa96bc>.
 24. Challenor J. - *Toxicology of Solvents*, Rapra Technology Ltd (2002). ISBN: 1-85957-296-0. <https://doi.org/10.1093/occmed/52.6.363-a>.
 25. Ho P. P., and Alfano R. R. - Optical Kerr effect in liquids, *Physical Review A* **20** (5) (1979) 2170-2187. <https://doi.org/10.1103/PhysRevA.20.2170>.
 26. Saitoh K., Florous N. J., and Koshiba M. - Theoretical realization of holey fiber with flat chromatic dispersion and large mode area: an intriguing defect approach, *Optics Letters* **31**(1) (2006) 26-28. <https://doi.org/10.1364/OL.31.000026>.
 27. Medjouri A., Simohamed L. M., Ziane O., Boudrioua A., and Becer Z. - Design of a circular

- photonic crystal fiber with flattened chromatic dispersion using a defected core and selectively reduced air holes: Application to supercontinuum generation at 1.55 μm . *Photonics and Nanostructures - Fundamentals and Applications* **16** (2015) 43-50. <https://doi.org/10.1016/j.photonics.2015.08.004>.
28. Moutzouris K., Papamichael M., Betsis S. C., Stavrakas I., Hloupis G., and D. Triantis. - Refractive, dispersive and thermo-optic properties of twelve organic solvents in the visible and near-infrared, *Applied Physics B* **116** (3) (2013) 617-622. <https://doi.org/10.1007/s00340-013-5744-3>.
 29. Kedenburg S., Vieweg M., Gissibl T., and Giessen H. - Linear refractive index and absorption measurements of nonlinear optical liquids in the visible and near-infrared spectral region, *Optical Materials Express* **2** (2012) 1588-611. <https://doi.org/10.1364/OME.2.001588>.
 30. Tan C. Z. - Determination of refractive index of silica glass for infrared wavelengths by IR spectroscopy, *Journal of Non-Crystalline Solids* **223** (1-2) (1998) 158-163. [https://doi.org/10.1016/s0022-3093\(97\)00438-9](https://doi.org/10.1016/s0022-3093(97)00438-9).
 31. Dhara P., and Singh V. K. - Investigation of rectangular solid-core photonic crystal fiber as temperature sensor, *Microsystem Technologies* **27** (2021) 127-132. <https://doi.org/10.1007/s00542-020-04927-1>.
 32. Agrawal G. P. - *Nonlinear Fiber Optics* (5th edition), Elsevier Academic Press (2013), ISBN: 9780123973078.
 33. Saitoh K., Koshihira M., Hasegawa T., and Sasaoka E. - Chromatic dispersion control in photonic crystal fibers: application to ultra-flattened dispersion, *Optics Express* **11**(8) (2003) 843-852. <https://doi.org/10.1364/OE.11.000843>.
 34. Begum F., Namihira Y., Kinjo T., and Kaijage S. - Supercontinuum generation in square photonic crystal fiber with nearly zero ultra-flattened chromatic dispersion and fabrication tolerance analysis, *Optics Communications* **284** (4) (2011) 965-970. <https://doi.org/10.1016/j.optcom.2010.10.029>.
 35. Van T. H., Kasztelaniec R., Anuszkiewicz A., Stepniewski G., Filipkowski A., Ertman S., Pysz D., Wolinski T., Khoa D. X., Klimczak M., and Buczynski R. - All-normal dispersion supercontinuum generation in photonic crystal fibers with large hollow cores infiltrated with toluene, *Optical Materials Express* **8** (11) (2018) 3568-3582. <https://doi.org/10.1364/OME.8.003568>.
 36. Vieweg M., Gissibl T., Pricking S., Kuhlmeier B. T., Wu D. C., Eggleton B. J., and Giessen H. - Ultrafast nonlinear optofluidics in selectively liquid-filled photonic crystal fibers, *Optics Express* **18**(24) (2010) 25232-25240. <https://doi.org/10.1364/OE.18.025232>.
 37. Van T. H., Kasztelaniec R., Filipkowski A., Stepniewski G., Pysz D., Klimczak M., Ertman S., Van C. L., Woliński T. R., Trippenbach M., Khoa D. X., Śmietana M., and Buczyński R. - Supercontinuum generation in an all-normal dispersion large core photonic crystal fiber infiltrated with carbon tetrachloride, *Optical Materials Express* **9**(5) (2019) 2264-2278. <https://doi.org/10.1364/OME.9.002264>.
 38. Nielsen K., Noordegraaf D., Sørensen T., Bjarklev A., and Hansen T. P. - Selective filling of photonic crystal fibers, *Journal of Optics A: Pure and Applied Optics* **7** (8) L13-L20 (2005). <https://doi.org/10.1088/1464-4258/7/8/L02>.